Korean J. Chem. Eng., 39(12), 3305-3314 (2022)
DOI: 10.1007/s11814-022-1253-6

pISSN: 0256-1115
eISSN: 1975-7220

Sb-Fe bimetallic non-aqueous phase desulfurizer for efficient absorption of hydrogen sulfide: A combined experimental and DFT study

Zhihao Liu*, Kui Qiu*,†, Yu Dong*, Zhaobo Jin*, Luwei Liu*, and Jirong Wu**

*School of Chemistry and Chemical Engineering, Chongqing University of Science and Technology, No. 20 Daxuecheng East Road, Shapingba District, 401331 Chongqing, China
**Sinopec Southwest Oil and Gas Branch, Chengdu, 611930 Sichuan, China
(*Received 31 May 2022 • Revised 8 August 2022 • Accepted 10 August 2022*)

Abstract−A non-aqueous phase (Sb/Fe/NMP) desulfurization system for the removal of hydrogen sulfide from natural gas was constructed by introducing $SbCl_3$ and $FeCl_3$ in a specific ratio into N-methylpyrrolidone (NMP). The desulfurizing agent and its sulfur product were characterized, and the absorption pattern of H_2S by the system was investigated by static desulfurization experiments. The results indicate that the desulfurizer's sulfur capacity can reach 16 g/L at room temperature and pressure, and that adding the optimum amount of water and appropriate temperature increase can assist to increase desulfurization efficiency. The system maintained a sulfur capacity level of more than 90% of the initial sulfur capacity after five consecutive desulfurization-regeneration cycles. XRD and XPS spectrogram revealed that the regenerated solid product was high purity sulfur. Sb^{3+} is a key component to ensure the effective absorption of H_2S. The presence of a moderate amount of Fe^{3+} can oxidize and absorb small amounts of H_2S and promote the oxidative regeneration of the system. In addition, we combined the obtained experimental data with density flooding theory (DFT) theoretical calculations to show that the effective coordination of Sb(III) with HS^- in the NMP environment is the main reason for the effective absorption of H_2S by the desulfurizer. NMP is not involved in the coordination absorption process of hydrogen sulfide.

Keywords: DFT, Hydrogen Sulfide Removal, NMP, $SbCl_3$, Solvent Effect

INTRODUCTION

H_2S is a common component of oil and gas processing [1]. Its presence not only endangers human health but also corrodes metal equipment; thus, it must be strictly removed. Wet oxidative desulfurization (WOD) is commonly used among many desulfurization technologies [2]. It is a class of desulfurization methods that oxidizing solutions with weak alkalinity absorb H_2S in the gas and selectively oxidize it to elemental sulfur. This method is widely used in small and medium-scale gas purification (Sulfur content <5 t/d) because of its simple and high purification degree. Typical representative processes include modified ADA method [3], complexed iron method [4], and PDS method [5]. However, the problems of complex desulfurization agent components, low sulfur capacity, easy degradation of chelating agent for long-term use, generation of a large amount of industrial wastewater, and impurity of sulfur products [6] limit the further large-scale utilization of this method.

Compared with the aqueous phase desulfurization system, most non-aqueous phase systems are selected from environmentally friendly and stable organic solvents. Many of these solvents are polar solvents with suitable physical solvent solubility for H_2S. In addition, some metal salts can improve solubility in polar solvents by solvent effects. As a result, some scholars have introduced metal salts that promote the absorption of hydrogen sulfide into organic solvents and achieved certain results. Guo [7] constructed a new non-aqueous desulfurization system by introducing Fe(II) and DMF solvent into Fe(III)-IL. The addition of DMF significantly reduced the viscosity and acidity of the system, accelerated the oxidation reaction of active Fe(III) and S^{2-}, and improved the desulfurization efficiency. Qiu [8] formulated Fe-IL and NMP solvents in a 5 : 5 ratio by volume to form a desulfurization solution. The addition of NMP effectively reduced the solution viscosity and corrosiveness and achieved a sulfur capacity of 0.42 g/L while maintaining a high degree of purification. Hua [9] developed an $FeCl_3$/NMP non-aqueous phase desulfurization system for H_2S absorption and regeneration by O_2. This system obtained a high desulfurization efficiency of 99.72% and a high-quality sulfur product without the use of specific ligands or a controlled pH, considerably simplifying the synthesis processes in comparison to Fe-IL production. The low solubility of $FeCl_3$ in NMP leads to its low sulfur capacity, which limits the promotion of its application for the removal of high concentrations of H_2S. However, the catalytic oxidation activity of NMP as a solvent with ligands and iron ions forming solvation complexes on H_2S has attracted our keen interest.

NMP is a polar non-protonic solvent with superior solubility for some metal salts and the ability to physically absorb H_2S and CO_2 on its own; thus, it acts as the primary solvent in our current experiment. Existing studies [10] have shown that, despite having a specific oxidative desulfurization capacity, the efficiency needs to be improved to meet industrial demand by adding iron salts only

†To whom correspondence should be addressed.
E-mail: 2020205053@cqust.edu.cn

to the organic solvent. Solid desulfurization agents usually include appropriate amounts of Cu, Zn, and Mn to improve the desulfurization efficiency, mainly with the help of these transition metal ions, and H_2S can quickly form insoluble metal sulfides to achieve desulfurization purposes [11]. We hope to find a metal salt that can quickly react with H_2S and dissolves easily in polar organic solvents to remove H_2S effectively. From the solubility product constants of sulfides, it is known that Ag, Cu, Zn, Sb, Cd, Sn, Hg, Pb, etc., can react rapidly with H_2S to generate insoluble sulfides. We finally chose $SbCl_3$ for the experiments after considering factors such as environmental protection and material prices, as well as our preliminary solubility and desulfurization experiments. The $SbCl_3$/NMP system displayed excellent desulfurization performance at ambient temperature and pressure, demonstrating the concept's viability. Interestingly, no solid sulfur production was observed throughout the desulfurization process, suggesting that the mechanism of action is distinct from that of the traditional wet oxidation method. To the best of our knowledge, Sb has not been applied in natural gas desulfurization. More importantly, few studies on the formation of dissolved complexes of metal salts in the organic phase for effective hydrogen sulfide absorption have been reported, and the mechanism of action remains unknown. For this reason, we investigated the relevant factors affecting the performance of desulfurization agents through static desulfurization experiments. A series of characterization analyses of the desulfurizing agent and its solid products proposed a possible mechanism of action of the system on hydrogen sulfide, and density flooding theory (DFT) calculations further confirmed our conclusions.

EXPERIMENTAL

1. Materials

Antimony trichloride (99%), ferric chloride hexahydrate (99%), N-methyl pyrrolidone (99.5%, Water≤50 ppm), $K_3[Fe(CN)_6]$ (≥99.5%), were purchased from Aladdin Biochemical Technology Co (Shanghai, China). All chemicals used were of analytical grade and without further purification. Hydrogen sulfide and carbon dioxide standard gases were purchased from Rio Tinto Gas Company (Chongqing, China) for desulfurization and selectivity experiments, respectively. Standard gas 1 (CO_2 15.00 mol%, N_2 85.00 mol%) CO_2 concentration=150,000 ppm; Standard gas 2 (H_2S 5.01 mol%, N_2 94.99 mol%) H_2S concentration=50,100 ppm.

2. Characterization

FTIR profiles were obtained by scanning the samples in the range of 4,000-650 cm^{-1} on a Tension27 infrared spectrometer. The thermal stability of the desulfurization fluid was tested from room temperature to 500 °C at 10 °C min^{-1} under nitrogen using an STA409F5 TGA thermogravimetric analyzer (Netzsch, Germany). H-NMR spectra were recorded at room temperature with a Bruker DRX 400 MHz type spectrometer (400 MHz), internally referenced to $CDCl_3$ in the tetramethylsilane signal. The dynamic viscosity of the desulfurizer was measured with a rotational viscometer (DV-II+, Brookfield). The structure of the regenerated sulfur samples was tested using a Nihon Rei SmartLab-9 X-ray diffractometer. The test conditions were: CuKα-ray source, operating voltage 40.0 kV, operating current 30.0 mA, scan rate 5°/min, scan range 10-80°.

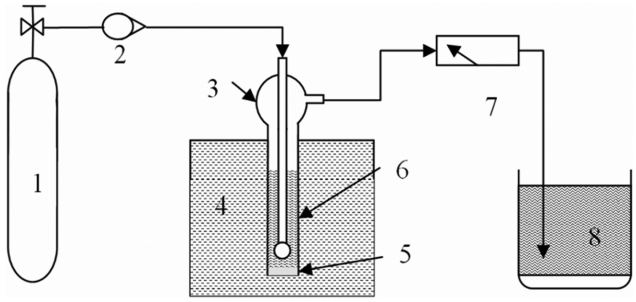

Fig. 1. Static desulfurization process.
1. H_2S/CO_2 gas cylinder
2. Flowmeter
3. Bubbling reactor
4. Temperature water bath
5. Sulfur precipitation
6. The desulfurization agent
7. H_2S detector
8. Saturated NaOH absorption solution

The different forms of elements in regenerated sulfur were determined by x-ray photoelectron spectrometry (XPS) on a Thermo Fisher Scientific K-Alpha instrument with Al Kα radiation (200 W). The binding energy (BE) was calibrated using the C1s line (284.8 eV). A Gauss-Lorentz peak was fitted to the XPS curve using the Advantage program.

3. Preparation of the Desulfurization Agent

To make organic desulfurization systems of various compositions, varying quantities of anhydrous $FeCl_3$ and $SbCl_3$ were added to 40 mL NMP and agitated at room temperature until they were entirely dissolved in the NMP solvent.

4. Desulfurization Experiment

The effect of solution composition, temperature, moisture content, and oxygen gas velocity on desulfurization and regeneration efficiency was investigated by desulfurization experiments. The static desulfurization experimental setup is shown in Fig. 1.

5. Evaluation of Gas Desulfurization

H_2S and CO_2 concentrations in the outlet gas stream were measured with an MSA portable multifunction detector (Methanex, Inc., USA). The temperature control range of the constant temperature water bath was 20-80 °C, the specification of the bubbling reactor was 3 cm in diameter and 15 cm in height, and the desulfurization solution was filled with 40 ml. All experiments were conducted at an ambient humidity of 20% after drying. Considering the presence of both physically dissolved and chemically absorbed H_2S in the desulfurization agent, the sulfur capacity is calculated as the following formula.

$$a = \frac{Q \times \left(t_1 \times C - \int_{t_2}^{t_1 - t_2} C' dt \right) \times M_{H_2S}}{1{,}000 \times V_m \times V} \quad (1)$$

where a is the sulfur capacity of the desulfurization agent, g/L; Q is the rate of raw gas entering the desulfurization device, mL/min; t_1 is the desulfurization time, min when the concentration of H_2S in the tail gas exceeds 20 ppm is the end of the experimental timing; c is the concentration of H_2S in the raw gas, %; t_2 is the time when H_2S appears in the tail gas, min; M_{H_2S} is the molar mass of H_2S, g/mol; V_m is the molar volume of gas, taken as 22.4 L/mol; V denotes the volume of the desulfurization agent, mL; C′ is the con-

centration of H_2S in the tail gas, C′ in this experiment not exceed 20 ppm, so C′ is much smaller than C, $\int_{t_2}^{t_1-t_2} C'dt$ is negligible and does not affect the final result.

6. Regeneration Experiment

The desulfurization solution was regenerated by the introduction of oxygen. Oxygen was continuously introduced into the saturated $FeCl_3/SbCl_3$/NMP system and the change in the appearance of the solution was observed, and the oxidation reduction potential (ORP) value of the system was measured every half hour. Using $K_3[Fe(CN)_6]$ titration, the system is considered to have fully regenerated when no more blue color is seen while oxygen is being continually fed to the bubble tube and no solids are still being created. The solid products were filtered and separated, the desulfurization solution was desulfurized again under the same conditions, and the experimental data were recorded; this process is regarded as a complete desulfurization-regeneration cycle.

7. Theoretical Calculation

Theoretical calculations were performed at the density functional theory (DFT) level of the Lee-Yang-Parr gradient-corrected correlation functional (B3LYP) hybrid functional [12,13] method and def2-TZVP [14,15] basis set using the Gaussian 09 D.01 software package [16]. Geometries for minima were optimized at the liquid phase, where the solvent effect of 1-methyl-2-pyrrolidinone (NMP, CAS. 872-50-4) was implicitly incorporated by utilizing the solvation model on density (SMD) [17]. The long-range van der Waals (vdW) interactions were considered by Grimme's DFT-D3 scheme [18]. Vibrational frequency was calculated to confirm that optimized structures possessed no imaginary frequency, i.e., they are located at the minima of the potential energy surface and yield the free energy, enthalpy, and entropy at 298.15 K 1 atm. The absorption energy was gained at the M06-2X [19]/def2-QZVP [14,15] level of theory, whose expression can be written as

$$E_{ads}=E(A-B)-E(A)-E(B) \quad (2)$$

The items on the right-hand side are the energies of dimer A-B, molecules A, and B, respectively. Electron localization function (ELF) [20] was gained from Multiwfn 3.8 [21], whose input files were extracted from Gaussian formatted checkpoint files at the M06-2X/def2-QZVP level of theory.

RESULTS AND DISCUSSION

1. Characterization of Desulfurization Agents

NMP and $FeCl_3/SbCl_3$ are completely miscible. The structural stability of the hybrid system is crucial for desulfurization. FTIR characterized the chemical structure of the desulfurizing agent. Fig. 2 shows that the C=O stretching vibration in NMP caused a clear stretching vibration absorption peak in the IR spectra at 1,675 cm^{-1} [22]. The addition of $SbCl_3$ to the NMP produced a new peak shape at 1,635 cm^{-1} attributable to the C=O--Sb coordination bond and a similar effect was observed with the addition of $FeCl_3$. The creation of oxygen-metal coordination bonds has previously been shown to cause a shift in the electronic energy band, lowering the C=O frequency [23]. The red shift of NMP is thought to be caused by the formation of C=O--Sb and C=O--Fe coordination bonds

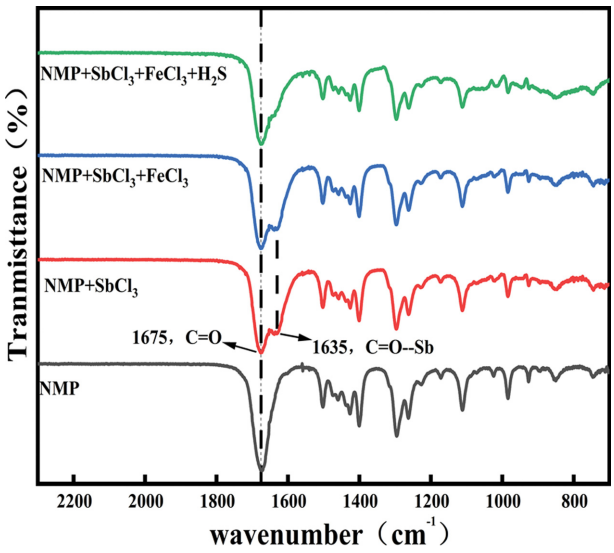

Fig. 2. IR spectrum of NMP, $SbCl_3$+NMP, $FeCl_3$+$SbCl_3$+NMP, NMP+$SbCl_3$+$FeCl_3$+H_2S.

between oxygen atoms and Sb^{3+} and Fe^{3+} in C=O. After the absorption of hydrogen sulfide by the desulfurization agent, the distinctive peaks of C=O--Sb vanished, indicating that the introduction of hydrogen sulfide broke the coordination between the original $SbCl_3$ and NMP molecules. However, the spectrum's shape after the absorption of hydrogen sulfide does not differ from that of NMP, which means that NMP is not further involved in the binding of H_2S.

H-NMR analysis was performed to further confirm the structure. Fig. 3 shows the NMR hydrogen spectra of NMP, NMP+

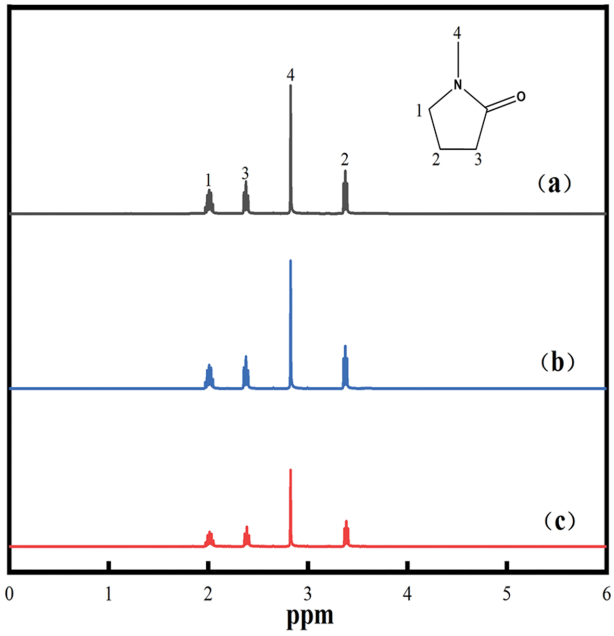

Fig. 3. H-NMR analysis of the desulfurization agent before and after absorption of H_2S. (a) NMP, (b) NMP+$SbCl_3$, (c) NMP+$SbCl_3$+H_2S.

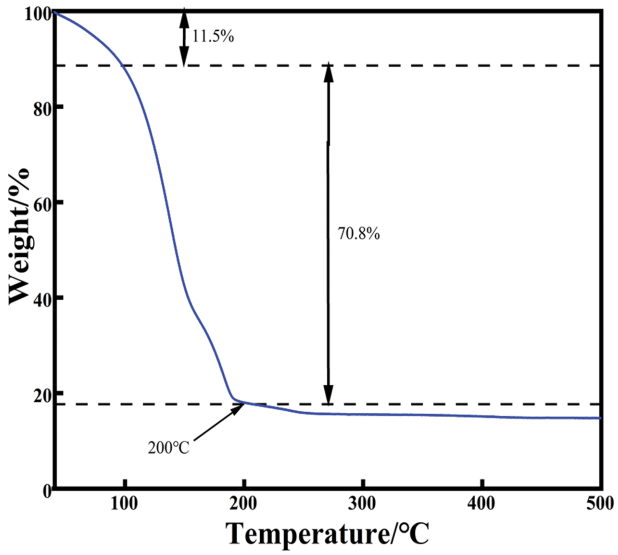

Fig. 4. TGA curve of the desulfurization agent.

$SbCl_3$, and NMP+$SbCl_3$+H_2S. Because the coordination bonds are weak covalent bonds, which are usually spatial interactions with low strength and do not change the electron cloud shape, the differences between NMP and NMP+$SbCl_3$ were not visible in the NMR spectra. Moreover, it is not difficult to find that the number and peak area of hydrogen in NMP+$SbCl_3$+H_2S are identical to those of NMP molecules, which indicates that the chemical environment of H on NMP molecules does not change before and after the absorption of hydrogen sulfide. Combined with the phenomena observed in the infrared spectra, it can be concluded that after the absorption of H_2S, the NMP in the system is in the free state, i.e., NMP is not involved in the chemical absorption of H_2S.

The thermal stability of the desulfurization system was evaluated using TGA, and its thermogravimetric curve is shown in Fig. 4. The TG picture of the desulfurization agent indicates that the desulfurization agent begins to lose weight at 50 °C and becomes serious after 100 °C. This is because NMP is highly hydrophilic and readily absorbs water [24], so the weight loss between 50 °C and 100 °C can be attributed to the evaporation of water absorbed by the desulfurizer from the air before the test, accounting for 11.5% of the total weight loss. Because NMP has a boiling point of 202 °C, weight loss is 70.8% between 100 °C and 200 °C due to NMP volatilization. After 200 °C, the continuous temperature increase causes the solvent to evaporate completely, the remaining solids should be Sb^{3+} and Fe^{2+} complexes with NMP, respectively [25]. From the overall view of the thermogravimetric curve, the actual desulfurization should try to control the temperature not to exceed 80 °C, which can make the trace water absorbed by NMP evaporate slowly and also prevent the oxidation and thermal evaporation of NMP.

The lower viscosity of the solution means less resistance to mass transfer of the gas in the solution, better mobility, and a faster absorption rate. The ionic liquid's excessive viscosity seriously affects the gas-liquid mass transfer effect, resulting in the sulfur capacity being much lower than its theoretical value [7]. To explore the variation of dynamic viscosity with temperature, the desulfurizing agent's dynamic viscosity was evaluated using a rotational viscometer, and the findings are presented in Table 1.

Table 1. The relationship between viscosity and temperature of desulfurizer

T/K	η/(mPa·s)		
	w_1	w_2	w_3
303.15	2.1	3.2	7.0
333.15	1.6	1.9	5.5
363.15	1.5	1.8	4.9

Notes: w_1-40 ml NMP; w_2-40 ml NMP+1 g $FeCl_3$; w_3-40 ml NMP+1 g $FeCl_3$+8 g $SbCl_3$

The results show that the viscosity of the Sb/Fe/NMP desulfurization agent is significantly lower than that of common ionic liquids reported in the literature [26], even after adding 8 g $SbCl_3$. Consequently, the Sb/Fe/NMP desulfurization agent can dissolve more $SbCl_3$ in the later stages of desulfurization agent synthesis, increasing desulfurization efficiency.

2. Desulfurization Agent Performance Evaluation

2-1. Factors Affecting H_2S Absorption

The effect of antimony content, temperature, flow rate, and moisture content on the purification efficiency of desulfurizer was investigated by static desulfurization experiments in a room environment with 20% humidity by adding 1 g $FeCl_3$ to 40 mL NMP and setting the raw gas H_2S concentration at 5.01% and flow rate at 30 mL/min.

As shown in Fig. 5(a), the absorption efficiency of H_2S is minimal when only 1 g $FeCl_3$ is added to 40 mL NMP at atmospheric pressure. The tail gas H_2S concentration exceeds the standard within 7 minutes, indicating that, while the $FeCl_3$/NMP system has some oxidative absorption capacity for H_2S, the absorption efficiency is low. Because the $FeCl_3$ addition reaches dissolution saturation after 1.2 g, it cannot be increased by increasing the $FeCl_3$ concentration to improve the solvent's desulfurization efficiency. As for the role played by Fe^{3+} in the absorption process, we clarified this by controlled experiments under the same conditions. It is not difficult to find that pure NMP cannot be effective in absorbing H_2S. The concentration of H_2S in the exhaust gas is already greater than 20 ppm in less than a minute, which indicates that NMP is more as a solvent, and the contribution of physical absorption of H_2S is very small. Before and after the addition of $FeCl_3$, the system maintained the purification degree for only a 4 minute difference. It is noteworthy that the $SbCl_3$/$FeCl_3$/NMP system gradually changed from colorless to yellowish after absorption of H_2S, and the presence of Fe^{2+} in the enrichment solution was detected by titration with $K_3[Fe(CN)_6]$. This indicates that Fe^{3+} does oxidize and absorbs part of H_2S, and the small amount of sulfur produced is dissolved in the solvent. Meanwhile, adding 1 g of $SbCl_3$ to the above desulfurizer, the tail gas $H_2S \leq 20$ ppm lasted for 62 min, and the desulfurization efficiency was significantly improved. With the increase of $SbCl_3$ addition, the time to maintain the strict purification of the desulfurization agent is basically proportional to the increase of $SbCl_3$ addition. This is due to the strong solvent effect of $SbCl_3$ by NMP, which leads to the high solubility of $SbCl_3$ in NMP [27]. Dissolved $SbCl_3$ provides a rich site of action for H_2S uptake and the two react rapidly, unlike the aqueous phase system where Fe^{3+}/

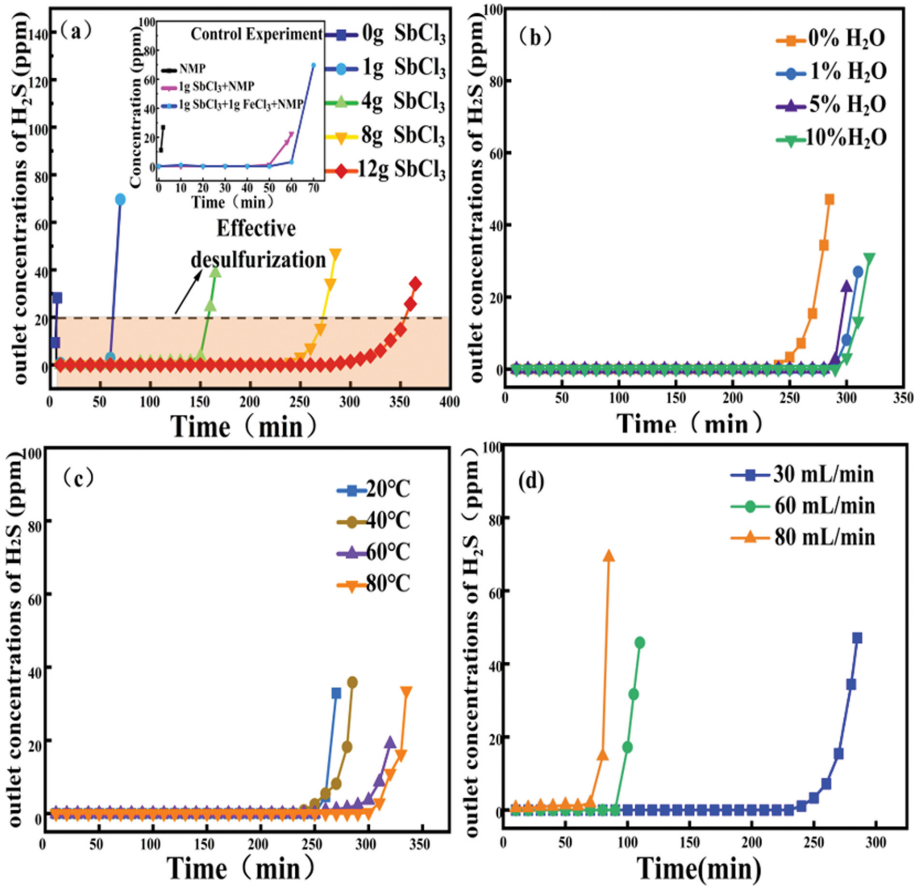

Fig. 5. Breakthrough curve of desulfurization agent under different conditions. (a) Effect of metal salt concentration on purification efficiency at 40 °C, (b) Effect of water content on desulfurization efficiency at 40 °C, (c) Effect of temperature on desulfurization efficiency, (d) Effect of flow rate on desulfurization efficiency (at 40 °C and 10% water content, inlet H_2S concentration=50,100 ppm).

Cu^{2+} reacts with H_2S to form FeS and CuS precipitates to achieve rapid desulfurization [28]. When $SbCl_3$ was added at a dosage of 8 g, the tail gas H_2S concentration was maintained at 0 for more than 250 min, corresponding to a sulfur capacity of 16 g/L. When 12 g of $SbCl_3$ was added, the effective purification time exceeded 350 minutes, showing that this desulfurizer's sulfur capacity level far exceeded that of the already reported ionic liquid and aqueous phase wet oxidation desulfurization systems [29]. The continued addition of $SbCl_3$ was still soluble in NMP solvent, and the length of time to maintain strict purification continued to be extended. Still, the solution viscosity gradually increased with salt added. It is not conducive to gas-liquid mass transfer absorption. Therefore, the subsequent experiments used the ratio of 40 ml NMP+1 g $FeCl_3$+ 8 g $SbCl_3$. Combined with the above experimental phenomena, we believe that Sb^{3+} is the critical component in ensuring the efficient absorption of H_2S. Fe^{3+} can oxidize and absorb part of H_2S. However, its contribution is much smaller than that of Sb, and there is no synergistic effect between Sb and Fe.

In the desulfurization operation, the desulfurizing agent inevitably brings in water. When water is introduced, the solvent is diluted, which on the one hand lowers the concentration of useful components. Alternatively, it might alter the solution's viscosity, which would have an impact on the effectiveness of the desulfurization process. Antimony chloride is very easy to hydrolyze in pure water to produce Sb_2O_3, but how will it change in organic solvents containing water? Furthermore, the complete desulfurization-regeneration cycle continuously converts H_2S to S and H_2O, with water accumulating as the cycle progresses. Therefore, it is necessary to study the effect of water content on the stability and desulfurization efficiency of desulfurization agents. It can be noticed that the desulfurization performance of the desulfurization agent increased by 10.7 percent ~14.2 percent over that of the desulfurization agent without water under the condition of adding a suitable amount of water. This is because adding a small amount of water can reduce the viscosity and acidity of the desulfurization agent, increasing the solubility and absorption efficiency of H_2S. When the water content is greater than 10%, the desulfurization agent gradually begins to precipitate a small amount of white solid, because Sb^{3+} is easily hydrolyzed to generate Sb_2O_3. Therefore, the H_2O content in the system should be kept within 10%, so that the performance can be improved without affecting the desulfurizer composition.

Fig. 5(c) shows that the desulfurization performance improves steadily as the temperature rises between 20 and 80 °C. Under 20 °C, the time it takes to maintain a rigorous degree of desulfurization can reach 260 minutes, showing that the degree of the desulfurization agent already has good capacity at that temperature. Desulfur-

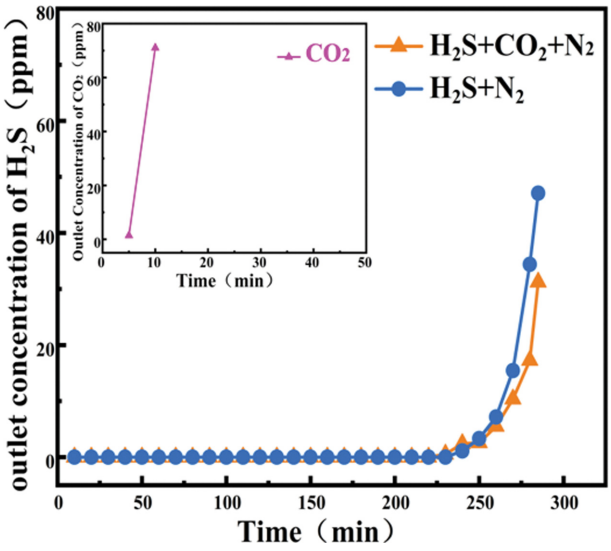

Fig. 6. Breakthrough curve of desulfurizer under different airflow composition.

ization to fulfill the strict purification time can be sustained for up to 300 minutes when the temperature increases to 80 °C. We found that with the gradual increase of temperature, the growth rate of the time to maintain the strict purification degree of the desulfurization agent is relatively slow. This is because the increasing temperature can further reduce the viscosity of the system to enhance gas-liquid transfer to enhance the desulfurization efficiency. However, due to the low viscosity of the desulfurization fluid itself, it can also be found from Table 1 that the temperature change has a small effect on its viscosity, so the desulfurization efficiency increases slightly by increasing the temperature.

Fig. 5(d) shows the breakthrough curve of the desulfurizer at different gas flow rates. The increase in gas flow rate reduces the absorption capacity because the retention time of the active ingredient of the desulfurizer interacting with H_2S decreases at higher flow rates. The sulfur capacity of the desulfurizer decays relatively slowly at low to high gas velocities of 14.80 g/L, 11.38 g/L, and 9.28 g/L, respectively.

2-2. Desulfurizer Selective Absorption

In practical industrial scenarios, impurity components in natural gas are often blended with different levels of CO_2 and N_2 in addition to H_2S. To study the performance of H_2S/CO_2 selective separation, selective absorption experiments were carried out in a mixture of H_2S, CO_2, N_2, and a mixture of H_2S and N_2, respectively. It can be seen from the Fig. 6 that the absorption capacity of the desulfurizer for CO_2 is very limited, and the CO_2 concentration in the tail gas has exceeded 20 ppm in about 8 minutes. The absorption part is mainly the physical absorption of CO_2 by the solvent NMP. In the presence of CO_2, the removal capacity of H_2S by the

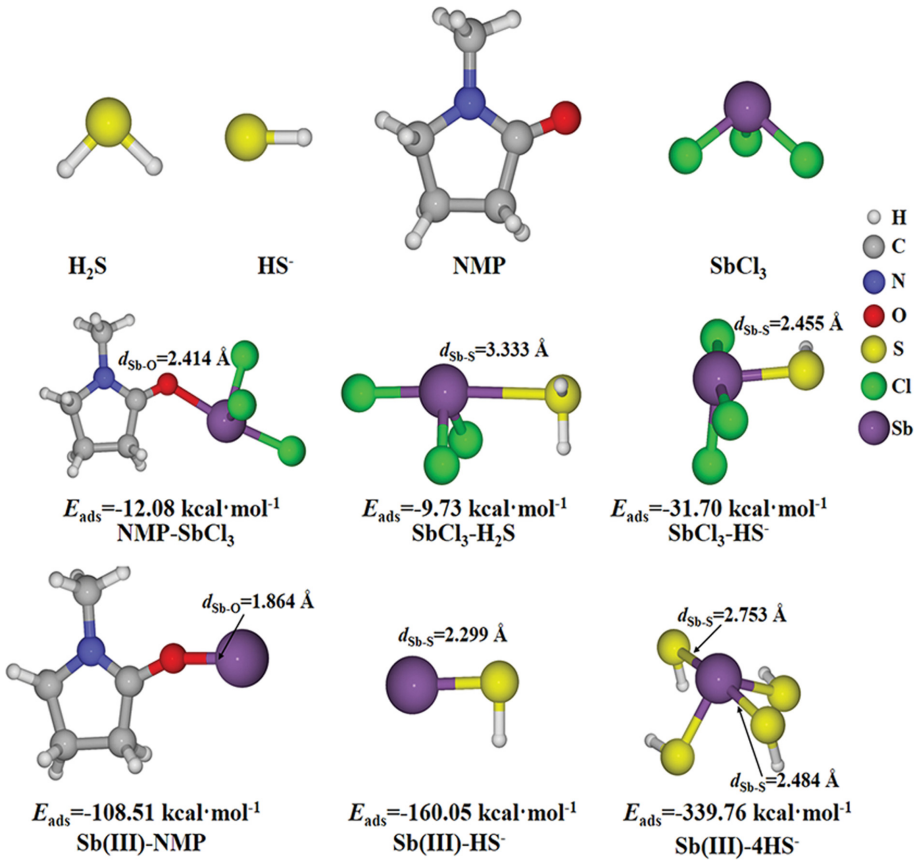

Fig. 7. The optimized structures of studied molecules, where the white, grey, blue, red, yellow, green, and purple colors denote H, C, N, O, S, Cl, and Sb atoms, and E_{ads} is the absorption energy (kcal·mol^{-1}).

desulfurizer did not change significantly. By calculating the absorption amount, it was found that the absorption amount of hydrogen sulfide by the desulfurizing agent in the mixture of H_2S, CO_2, N_2 and the mixture of H_2S and N_2 was 15.79 g/L and 15.56 g/L, respectively. The above experimental results show that the desulfurizer has almost no absorption capacity for CO_2, and the desulfurizer can still maintain the efficient removal of H_2S under the interference of CO_2.

3. Computational Chemical Analysis of Desulfurization Reaction

Density functional theory (DFT) is a useful tool for analyzing the functional groups and the interactions among system components [30,34]. From the IR and NMR spectra, we conclude that NMP only acts as a solvent, forming a complex with $SbCl_3$ and is not involved in the chemical absorption of hydrogen sulfide. This may be due to the fact that the NMP molecule as a ligand is not stable [31] and the S in the hydrogen sulfide molecule is more strongly coordinated to Sb(III) than O. Therefore, S as a Lewis soft base and Sb as a Lewis acid are more inclined to interact and form a stronger Sb-S coordination bond [32,33]. To prove this conjecture, the absorption between NMP and $SbCl_3$ as well as $SbCl_3$ and H_2S was investigated in this study by DFT calculations, and the possible monomers and dimers present in the system are shown in Fig. 7.

The Sb atom can interact with the O atom in NMP and S atom in H_2S, whose bond lengths are 2.414 Å and 3.333 Å. In terms of absorption energy, E_{ads} (NMP-$SbCl_3$)=−12.08 kcal/mol is greater than E_{ads} ($SbCl_3$-H_2S)=−9.73 kcal/mol), indicating that the conformation of NMP-$SbCl_3$ is more stable than that of $SbCl_3$-H_2S. However, the experiment has verified that $SbCl_3$ is preferential to H_2S over the NMP, not aligning with the calculation results above. What is the reason for this contradiction? We speculate that H_2S does not easily exist in molecular form in the NMP solvent but ionizes as HS^- to participate in the competition for the (NMP-$SbCl_3$) coordination reaction. As a strong polar and Lewis base, NMP induces H_2S to form δ+H-δ-SH, which promotes the ionization of H_2S [7]. Thus, we have optimized the structure of $SbCl_3$-HS^- as shown in Fig. 9, whose absorption is −31.70 kcal/mol, demonstrating that the calculation result matches the experiment result. Still, the Sb-S bond length (2.455 Å) is longer than the Sb-O one (2.414 Å), but if we consider the atomic van der Waals radii [18] (Sb: 2.06 Å, S: 1.80 Å, O: 1.52 Å), it can be found that the overlap extent of Sb-S is larger than Sb-O. Considering that metal salts are ionized by solvation in polar solvents [34] and that Sb(III) in the system can interact with not only one HS^- in NMP solvents, we also calculated classical conformations of Sb(III)-4HS^- molecules with absorption energies of −339.76 kcal·mol^{-1}, which indicates that Sb can indeed bind to HS^- molecules, thus being the reason for the experimental ability of Sb to absorb H_2S. For Sb(III)-NMP molecule, the

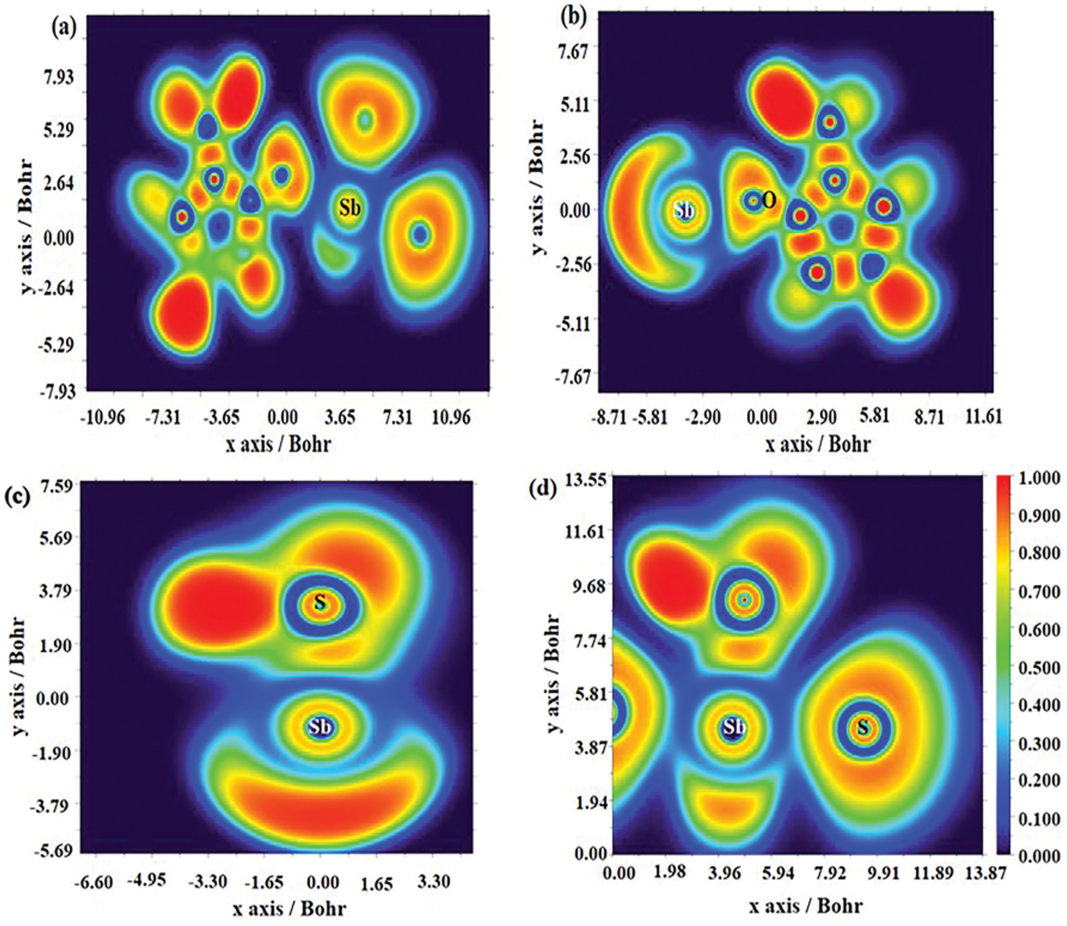

Fig. 8. The ELF snapshots for NMP-$SbCl_3$ (a), Sb(III)-NMP (b), Sb(III)-HS^- (c), and $SbCl_3$-HS^- (d) molecules at Sb-S and Sb-O planes, respectively.

Table 2. Reactivity Gibbs free energy (ΔG) of NMP-$SbCl_3$, $SbCl_3$-HS^-, Sb(III)-, NMP, and Sb(III)-HS^- molecules at different temperatures

T/K	ΔG (kcal/mol)			
	NMP-$SbCl_3$	$SbCl_3$-HS^-	Sb(III)-NMP	Sb(III)-HS^-
273	0.628	−30.120	−112.633	−175.211
303	1.883	29.493	−111.733	−174.672
333	3.138	−27.610	−110.915	−173.521

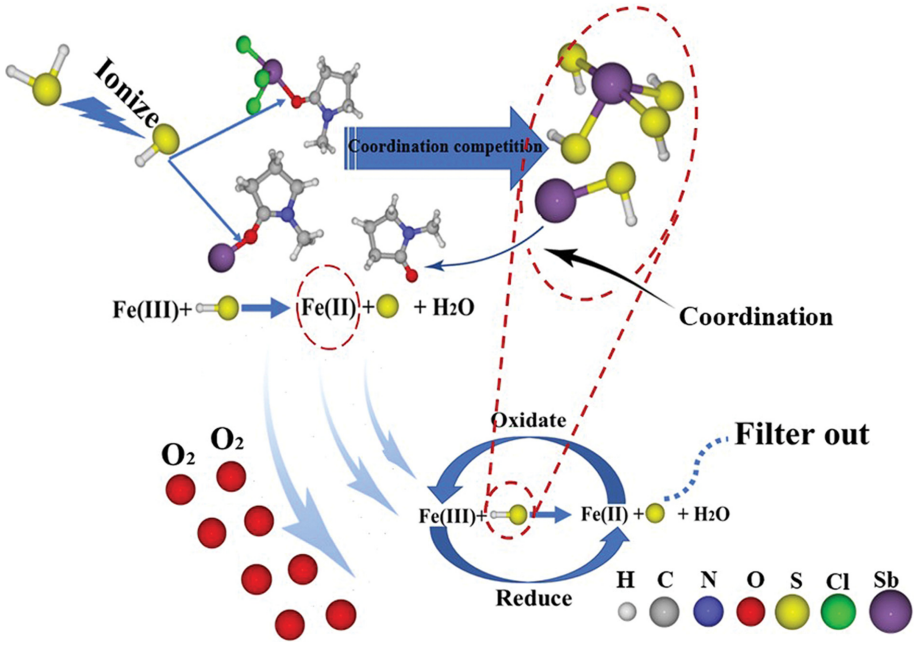

Fig. 9. A possible mechanism of desulfurization and regeneration for the Sb/Fe/NMP system.

Sb-O bond length, and absorption energies are 1.864 Å and −108.51 kcal·mol^{-1}, which is shorter and larger than the bond lengths and average absorption energy for Sb(III)-4HS^- (−84.94 kcal·mol^{-1}). However, this does not imply that Sb has a greater advantage in terms of absorption effect for NMP than HS^- because NMP has a strong steric effect and has a minimal coordination number with Sb(III). The absorption energy of Sb(III)-HS^- is −160.05 kcal·mol^{-1}, which is more negative than the Sb(III)-NMP and explains why Sb(III) can absorb HS^-.

The reactive Gibbs free energy of the studied molecules at different temperatures is listed in Table 2. Note that NMP-$SbCl_3$ has positive reactive Gibbs free energy. In contrast, $SbCl_3$-HS^-, Sb(III)-HS^-, and Sb(III)-NMP have negative reaction Gibbs free energies. Thus, Sb(III)-HS^- is thermodynamically more favorable than Sb(III)-NMP in terms of ΔG magnitude [35]. To further elucidate the electronic localization of the Sb-O and Sb-S bonds, we investigated the ELF of the above dimer, as shown in Fig. 8. From the color in ELF snapshots, the order extent of electron localization is Sb-S in Sb(III)-HS^->Sb-O in Sb(III)-NMP>Sb-S in $SbCl_3$-HS^->Sb-O in $SbCl_3$-NMP, which is in line with the above calculations of bond length and absorption energy.

Combining the experimental phenomena and theoretical calculations, the possible desulfurization and regeneration mechanism of the Sb/Fe/NMP system is proposed as shown in Fig. 9, NMP acts as a strong polar non-protonic solvent and relies on the solvent effect to dissolve $SbCl_3$ in large amounts, and $SbCl_3$ or Sb^{3+} dissolved in the organic phase can form spatial steric complexes with oxygen atoms on C=O in NMP. When H_2S molecules are dissolved in the desulfurizer's liquid phase and ionized into HS^- by the NMP solvent's good physical solubility, they replace the coordination bonds formed by C=O and Sb in the original NMP due to the stronger coordination bonds between S and Sb and react rapidly to form the more stable $[Sb(HS^-)_n]^{(3-n)+}$ coordination structure. Furthermore, recent research has revealed that the stability of covalent coordination bonds rises dramatically with increasing solvent polarity [36], implying that Sb-S coordination bonds are more stable in the NMP environment. The Fe^{3+} dissolved in NMP directly reacts with HS^- in a redox reaction, and the small amount of S generated is dissolved in NMP, and Fe^{2+} continues to exist in the system by forming complexes with NMP [30]. When the desulfurizer is regenerated with the participation of oxygen, on the one hand, the Fe^{2+} in the system is re-oxidized to Fe^{3+}, and Fe^{3+} rapidly oxidizes HS^- in the coordination state to generate S. On the other hand, Sb(III) recombines with NMP to form the original complex to achieve rapid regeneration. The reduced Fe^{2+} continues to be oxidized to Fe^{3+} by oxygen, and so on until the absorbed H_2S is completely converted to S. The desulfurization agent absorption process is characterized by high mass transfer efficiency

due to the low viscosity of the system; the dissolution of H_2S and the formation of complexes with Sb(III) are fast reactions, which determines the high efficiency of this desulfurization system to absorb H_2S.

4. Study on the Regeneration Performance

The regeneration ability of desulfurization agents can reduce regeneration time, increase solution circulation efficiency, and reduce energy consumption and solution loading. To assess its potential for practical application, the cycling performance of the adsorbent was investigated. 1 g of $FeCl_3$ was added to the $SbCl_3$/NMP-enriched solution that had absorbed H_2S. Additionally, oxygen was continuously introduced to the solution to observe any changes in the solution's appearance, and the system's oxidation reduction potential (ORP) value was measured every half-hour. Fig. 10(a) shows that the ORP value of the rich solution starts from 48 mV. The electrode potential rises rapidly to 392 mV and 409 mV, respectively, after 1 h of continuous oxygenation. The ORP value of the solution with continued oxygenation stabilizes, which indicates that the small amount of Fe^{3+} in the desulfurization agent under oxygenation conditions is sufficient to oxidize the vast majority of H_2S to S within 1 h to achieve complete regeneration. With time, the color of the solution gradually changes from clear to turbid yellow, indicating that sulfur was steadily produced. Fig. 10(b) illustrates that after five desulfurization-regeneration cycles, the desulfurizer remains strictly purified for more than 265 minutes, maintaining about 90% of the first desulfurization.

Fig. 11(a) and 11(b) show the XRD and XPS spectra of the products obtained by regenerating the desulfurizer, respectively. A comparison of the spectra in Fig. 11(a) with the XRD standard pattern library shows that the characteristic diffraction peaks of the products are all consistent with the -sulfur standard pattern PDF#78-1889, indicating the presence of sulfur in the desulfurized products. Furthermore, a comparison of this desulfurization product with conventional XRD patterns of metallic sulfur-containing com-

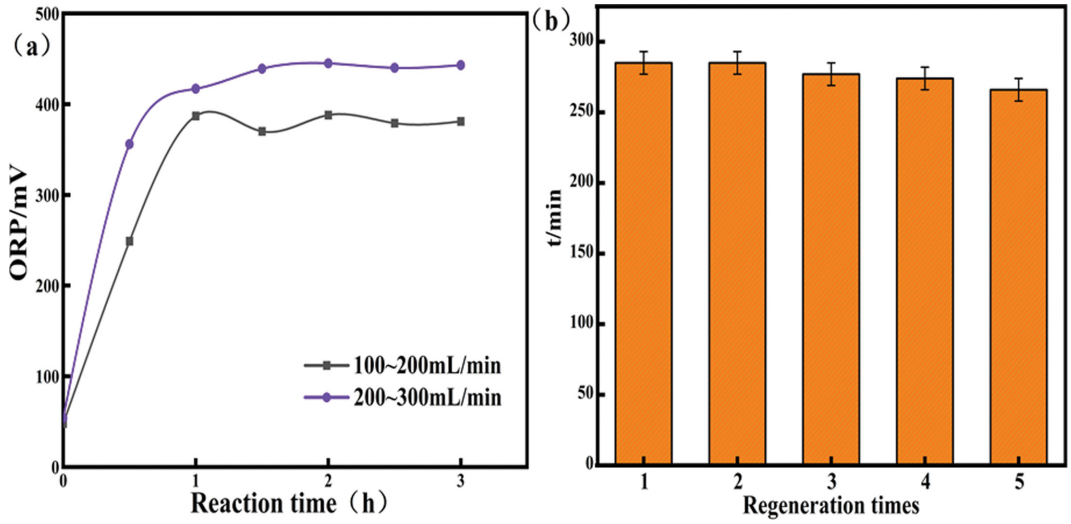

Fig. 10. (a) Variation of ORP value with time under different oxygen gas rate regeneration; (b) Variation of the time to maintain the purification of the desulfurization reaction with the number of desulfurization-regeneration cycles.

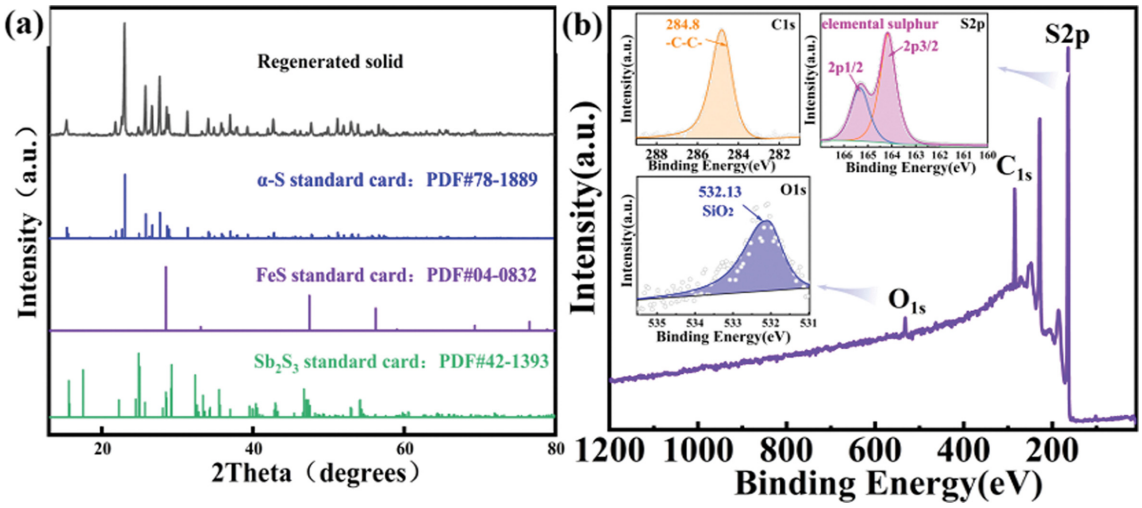

Fig. 11. (a) XRD spectrogram of sulfur products; (b) XPS spectrogram of sulfur products.

pounds such as FeS and Sb_2S_3 found that it lacks the distinctive diffraction peaks of iron sulfide and antimony sulfide, showing that the product is highly pure sulfur. This is further confirmed by the XPS results. The full spectrum of the solid product shows that it contains the elements S, O, and C. A fit to the single scan spectra of C and O shows that all O and C elements in the product are from contamination in the external environment and do not contain oxides of sulfur. A split peak fit to the single scan spectrum of S shows that the peak positions at 164.1 eV and 165.3 eV can be attributed to the 2p3/2 and 2p1/2 orbitals of elemental sulfur, respectively, without the inclusion of other sulfur species, which is consistent with that reported in the literature [37]. The above results show that the desulfurizer regeneration performance is good and the reproduced product is high purity sulfur.

CONCLUSION

The Sb/Fe-NMP system was used as an efficient absorber for capturing H_2S. The system exhibits better sulfur capacity levels (up to 16 g/l at ambient temperature and pressure) than reported in the literature for absorbents so far. In addition, the system has low viscosity, good chemical and thermal stability, and can be rapidly regenerated by continuous oxygenation of the desulfurization enrichment, with the sulfur capacity remaining at more than 90% of the initial sulfur capacity after five cycles of repeated use. The efficient absorption of H_2S by Sb/NMP relies on the rapid coordination between Sb(III) and H_2S molecules in the NMP environment to form a new $[Sb(HS^-)_n]^{(3-n)+}$ complex structure. The process is a chemical absorption process, and Sb is an effective component for efficient H_2S capture by the desulfurizer. This system is cheaper, easier to synthesize, and does not require purification than conventional ionic liquids and wet oxidation systems. Thus, this system could be a promising class of adsorbents for removing H_2S from natural gas with medium to high sulfur content at room temperature.

ACKNOWLEDGEMENT

The research was funded by China National Science and Technology Major Project (2016ZX05017) and Sinopec Group Corporation 2020 Science and Technology Project "Organic Sulfur Catalytic Hydrolysis Technology Improves Quality Research" (No. 120049-1).

CONFLICT OF INTEREST

The authors declare that they have no known competing financial interests or personal relationships that could have appeared to influence the work reported in this paper.

REFERENCES

1. M. Chen and Q. Cui, *Pet. Eng. Construction*, **36**, 1 (2010).
2. Y. Liu and Y. Wang, *Energy Fuels*, **33**, 10812 (2019).
3. D. Wu, J. Zhou, T. Yu, S. Wu and Y. Yang, *Chin. J. Environ. Eng.*, **7**, 3153 (2013).
4. Y. Zhao, J. Wang, Y. Liu, P. Zheng and B. Hu, *Environ. Res.*, **200**, 111423 (2021).
5. X. Zeng, X. Xiao, J. Chen and H. Wang, *Appl. Catal. B: Environ.*, **248**, 573 (2019).
6. F. Liu, J. Yu, A. B. Qazi, L. Zhang and X. K. Liu, *Environ. Sci. Technol.*, **55**, 1419 (2021).
7. Z. Guo, T. Zhang, T. Liu, J. Du, B. Jia, S. Gao and Y. Jiang, *Environ. Sci. Technol.*, **49**, 5697 (2015).
8. A. Patah, J. Bchle and G. Grampp, *J. Electrochem. Soc.*, **166**, H635 (2019).
9. G. Hua, Q. Zhang, D. Mcmanus, A. M. Z. Slawin and J. D. Woollins, *Dalton Trans.*, **9**, 1147 (2006).
10. J. H. Yang, *Korean J. Chem. Eng.*, **38**, 674 (2021).
11. X. Li, J. Han, Y. Liu, Z. Dou and T. A. Zhang, *Sep. Purif. Technol.*, **281**, 119849 (2022).
12. C. Lee, W. Yang and R. G. Parr, *Phys. Rev. B*, **37**, 785 (1988).
13. A. D. Becke, *Chem. Phys.*, **98**, 5648 (1993).
14. F. Weigend and R. Ahlrichs, *Phys. Chem. Chem. Phys.*, **7**, 3297 (2005).
15. F. Weigend, *Chem. Phys.*, **8**, 1057 (2006).
16. M. J. Frisch, G. W. Trucks and H. B. Schlegel, Gaussian Rev. D.01, Gaussian, Inc., Wallingford CT (2013).
17. A. V. Marenich, C. J. Cramer and D. G. Truhlar, *J. Phys. Chem. B.*, **113**, 6378 (2009).
18. S. Grimme, S. Ehrlich and L. Goerigk, *J. Comput. Chem.*, **32**, 1456 (2011).
19. Y. Zhao, N. E. Schultz and D. G. Truhlar, *J. Chem. Theory Comput.*, **2**, 364 (2006).
20. A. D. Becke, *J. Chem. Phys.*, **92**, 5397 (1990).
21. T. Lu and F. Chen, *J. Comput. Chem.*, **33**, 580 (2012).
22. G. Audran, E. G. Bagryanskaya and S. Marque, *Polymers*, **12**, 1481 (2020).
23. F. T. Li, B. Wu and R. H Liu, *Chem. Eng. J.*, **274**, 192(2015).
24. Y. J. Ou, X. M. Wang and C. L. Li, *IOP Conference Series Earth and Environmental Science 2017*, **100**, 12036 (2015).
25. G. Zhong, G. Mei and Y Jia, *Adv. Mater. Res.*, **549**, 126 (2012).
26. L. D. Cao, S. J. Zeng, X. P. Zhang and S. J. Zhang, *J. Chem. Eng.*, **66**, 1 (2015).
27. D. X. Wang, J. J. Ru and H. M. Huang, *Wet Metallurgy*, **40**, 4 (2021) (In Chinese).
28. X. Liu and R. Wang, *Fuel Process. Technol.*, **160**, 78 (2017).
29. A. H. Jalili, M. Mehrabi and A. T. Zoghi, *Fluid Phase Equilib.*, **453**, 1 (2017).
30. K. Ding, F. Zannat, C. J. Morris, W. W. Brennessel and P. L. Holland, *J. Org. Chem.*, **694**, 4204 (2009).
31. D. Amoroso and S. Picozzi, *Phys. Rev. B*, **93**(21), 214106 (2016).
32. G. Q. Zhong, M. Gu and Y. Q. Jia, *Adv. Mater. Res.*, **549**, 126 (2012).
33. H. Xu, D. Lee and J. He, *Phys. Rev. B*, **78**, 174103 (2008).
34. Z. Y. Yang, X. M. Liu and W. D. Yang, *J. Anal. Testing*, **3**, 19 (1992). (In Chinese).
35. M. J. Han, J. Y. He, W. Sun, S. Li and H. Yu, *Trans. Nonferrous Metals Soc. China*, **1**, 1 (2022).
36. R. Lo, D. Manna, M. Lamanec, M. Dračínský, P. Bouř, T. Wu, J. Kaleta and P. Hobza, *Nat. Commun.*, **13**, 1 (2022).
37. M. A. Hampton, C. Plackowski and A. V. Nguyen, *Langmuir*, **27**, 4190 (2011).